

# A quasi-time-dependent radiative transfer model of OH 104.9+2.4<sup>\*</sup>

D. Riechers<sup>1,2</sup>, Y. Balega<sup>3</sup>, T. Driebe<sup>2</sup>, K.-H. Hofmann<sup>2</sup>, A. B. Men'shchikov<sup>4</sup>, V. I. Shenavrin<sup>5</sup>, and G. Weigelt<sup>2</sup>

<sup>1</sup> Max-Planck-Institut für Astronomie, Königstuhl 17, 69117 Heidelberg, Germany  
e-mail: riechers@mpia-hd.mpg.de

<sup>2</sup> Max-Planck-Institut für Radioastronomie, Auf dem Hügel 69, 53121 Bonn, Germany

<sup>3</sup> Special Astrophysical Observatory, Nizhnij Arkhyz, Zelenchuk district, Karachai-Cherkessian Republic, Russia

<sup>4</sup> Institute for Computational Astrophysics, Saint Mary's University, Halifax, NS B3H 3C3, Canada

<sup>5</sup> Crimean Astrophysical Observatory, Nauchny, 98409, Crimea, Ukraine

Received 7 October 2004 / Accepted 8 February 2005

**Abstract.** We investigate the pulsation-phase dependent properties of the circumstellar dust shell (CDS) of the OH/IR star OH 104.9+2.4 based on radiative transfer modeling (RTM) using the code DUSTY. Our previous study concerning simultaneous modeling of the spectral energy distribution (SED) and near-infrared (NIR) visibilities (Riechers et al. 2004) has now been extended by means of a more detailed analysis of the pulsation-phase dependence of the model parameters of OH 104.9+2.4. In order to investigate the temporal variation in the spatial structure of the CDS, additional NIR speckle interferometric observations in the  $K'$  band were carried out with the 6 m telescope of the Special Astrophysical Observatory (SAO). At a wavelength of  $\lambda = 2.12 \mu\text{m}$  the diffraction-limited resolution of 74 mas was attained. Several key parameters of our previous best-fitting model had to be adjusted in order to be consistent with the newly extended amount of observational data. It was found that a simple rescaling of the bolometric flux  $F_{\text{bol}}$  is not sufficient to take the variability of the source into account, as the change in optical depth  $\tau$  over a full pulsation cycle is rather high. On the other hand, the impact of a change in effective temperature  $T_{\text{eff}}$  on SED and visibility is rather small. However, observations, as well as models for other AGB stars, show the necessity of including a variation of  $T_{\text{eff}}$  with pulsation phase in the radiative transfer models. Therefore, our new best-fitting model accounts for these changes.

**Key words.** radiative transfer – stars: AGB and post-AGB – stars: mass-loss – stars: circumstellar matter – infrared: stars – stars: individual: OH 104.9+2.4

## 1. Introduction

OH 104.9+2.4 (IRAS 22177+5936, AFGL 2885, NSV 25875, IRCO 243) is an OH/IR type II-A class star. Such objects are highly evolved asymptotic giant branch (AGB) stars exhibiting dusty envelopes, which are believed to be the main source of dust grains in our Galaxy. While the peak of the SED is expected to be around 6–10  $\mu\text{m}$  for OH/IR stars, the SiO and SiO<sub>2</sub> features at 9.7  $\mu\text{m}$  and 18  $\mu\text{m}$  are usually found in absorption, indicating a high optical depth of the CDS. This is consistent with the high mass-loss rates ( $10^{-7}$ – $10^{-4} M_{\odot}/\text{yr}$ , Habing 1996) that have been measured for these long-period variables (LPV). A large number of observational constraints were found for this class of stars, leading to detailed models of the evolution of these objects and the properties of their CDS (see Riechers et al. 2004, hereafter Paper I, and references therein). For OH 104.9+2.4, an outflow velocity of  $v_e = 15 \text{ km s}^{-1}$  was measured by te Lintel Hekkert et al. (1991), and the absolute distance was determined to be  $D = 2.38 \pm 0.24 \text{ kpc}$

(Herman & Habing 1985). From IR observations, we derived a pulsation period of  $P = 1500 \pm 11 \text{ d}$ , as well as a bolometric flux ranging from  $F_{\text{bol}} = 0.7 \times 10^{-10} \text{ W/m}^2$  at minimum phase to  $F_{\text{bol}} = 2.3 \times 10^{-10} \text{ W/m}^2$  at maximum phase (see Paper I for details).

The purpose of the present paper is to discuss our improved best-fitting radiative transfer model of OH 104.9+2.4. The paper is organized as follows: in Sect. 2, results of our new NIR speckle interferometric observations are presented. Sections 3.1 and 3.2 summarize the results of our best-fitting models from Paper I (hereafter model M-I) and our new best-fitting model (hereafter model M-II). Section 3.3 tests the model M-II quantitatively by comparing it with the SED data collected in Paper I for different pulsation phases. Section 4 summarizes and evaluates the results and closes the discussion with an outlook on future research.

## 2. Speckle interferometric observations and data reduction

In addition to our speckle interferometric observations in 2002, which were presented in Paper I,  $K'$ -band speckle

<sup>\*</sup> Based on data collected at the 6 m BTA telescope of the Special Astrophysical Observatory.

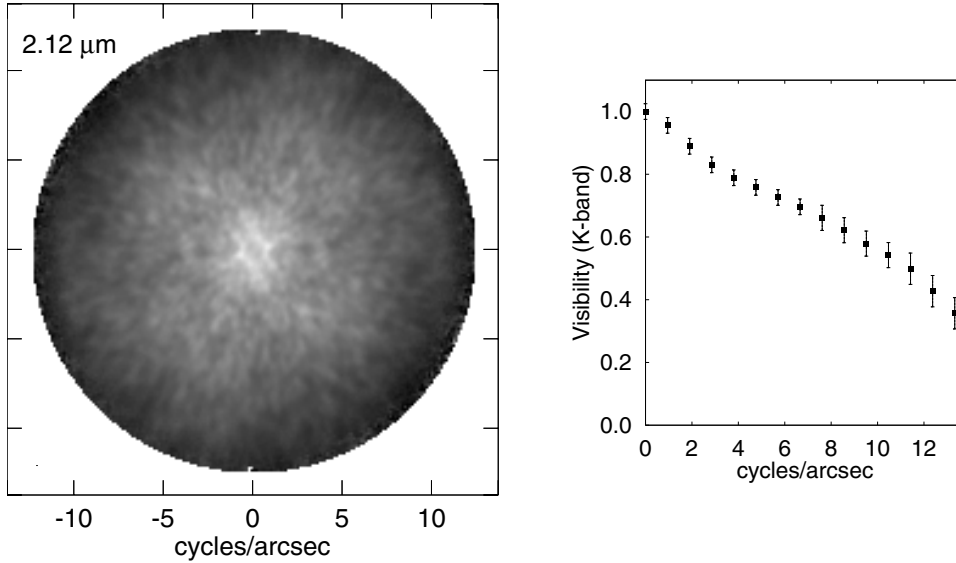


**Fig. 1.** Observations of OH 104.9+2.4 on October 11, 2003, with the SAO 6 m telescope. *Left:* 2-dimensional visibility function of OH 104.9+2.4 at 2.12  $\mu\text{m}$ . *Right:* azimuthally averaged visibility of OH 104.9+2.4 in the  $K'$  band.

interferograms of OH 104.9+2.4 were obtained with the Russian 6 m telescope of the Special Astrophysical Observatory on October 11, 2003. The data were recorded with our HAWAII speckle camera through an interference filter with a center wavelength of 2.12  $\mu\text{m}$  and bandwidth of 0.21  $\mu\text{m}$  ( $K'$  band). Additional speckle interferograms were taken for the unresolved reference star 2MASS J22191350+5949584. With a pixel size of 28.7 mas and seeing of 2.6 arcsec, 4100 object frames and 4600 frames of the reference star were taken, each with an exposure time of 218 ms. These interferograms were used to compensate for the speckle interferometry transfer function. The  $K'$ -band visibility function of OH 104.9+2.4 was derived from the speckle interferograms using the speckle interferometry method (Labeyrie 1970). The reconstructed two-dimensional visibility at 2.12  $\mu\text{m}$  and azimuthally averaged visibility profile are shown in Fig. 1. Given the accuracy and resolution of our visibility measurements, we find that the diameter ratio between major and minor axes differs from unity by less than 6%, which justifies the assumption of spherical symmetry.

From the pulsation period derived for OH 104.9+2.4 in Paper I, the phase of observations presented in this paper is determined to be  $\Phi^{2003} = 0.25$ , as compared to the phase of the 1996 ISO spectrum ( $\Phi^{\text{ISO}} = 0.5$ ) and to the phase corresponding to the 2002 SAO visibility measurements ( $\Phi^{2002} = 0$ ). Taking into account the uncertainties in the pulsation period caused by the low number of photometric data points and the resulting limitation to a rather simple fitting procedure, we estimate the total error of these phases to be  $\sim 0.02$ .

### 3. Dust shell models

#### 3.1. Previous results: Model M-I

As reported in Paper I, for the previous analysis of the radiative transfer in the CDS of OH 104.9+2.4,  $\sim 10^6$  models were calculated. To provide a reference for our SED model computations we used the 1996 ISO spectrum, while information about the spatial structure was given by our 2002 SAO  $K'$ -band

visibility. To simultaneously fit the SED and visibility data (i.e. with otherwise identical model parameters),  $F_{\text{bol}}$  was adjusted for the epoch of the visibility measurements with respect to the SED model, since the ISO spectrum and the 2002 visibility data were taken at different pulsation phases of OH 104.9+2.4. Therefore, M-I consists of an SED model where the bolometric flux was calculated from the 1996 ISO spectrum and from a visibility model using a bolometric flux for the 2002 SAO phase, which was derived from photometric measurements by different authors (see Paper I, Sect. 3). With these observational constraints and phase dependencies, we have found a model that fits the observations. The main parameters of M-I are summarized in Table 1.

#### 3.2. The new best-fitting model: M-II

Based on the new constraints given by the 2003 SAO visibility, some changes to M-I had to be introduced. The most significant change is that in addition to adjusting  $F_{\text{bol}}$ , a phase-dependent optical depth had to be introduced in order to be able to explain the observations. This approach was recently suggested based on analysis of the depth of the 9.7  $\mu\text{m}$  feature for other OH/IR stars (see Suh 2004, and references therein). In addition, the new model considers variations in the effective temperature of the central star, which is a less sensitive model parameter than the optical depth. All results for M-II are summarized in Table 2. The final model is shown in Fig. 2.

##### 3.2.1. Step 1: Improved SED fit

Apart from the goal of obtaining a good fit for multiple pulsation phases, another aim of the ongoing research was to find a dust type that is capable of reproducing, in particular, the 18  $\mu\text{m}$  absorption feature better than the dust composition used in M-I. Therefore, we included in our analysis several dust types not inherent to the DUSTY code (Ivezić et al. 1999) in order to widen our parameter space grid. The only dust type that was found to reproduce the SED of OH 104.9+2.4 significantly better than

**Table 1.** The derived and adopted physical parameters of OH 104.9+2.4 as provided by Model M-I.

| Parameter                          | Value   |
|------------------------------------|---|
| Effective temperature (black-body) | $T_{\text{eff}} = 2500 \pm 500$ K   |
| Temperature at inner CDS boundary  | $T_{\text{in}} = 1000 \pm 200$ K  |
| Density profile within the CDS     | $\rho(r) \propto r^{-n}$ with $n = 2.0 \pm 0.1$   |
| Relative CDS thickness             | $\frac{r_{\text{out}}}{r_{\text{in}}} = 10^p$ with $p = 5_{-2}^{+\infty}$   |
| Dust-grain distribution function   | MRN, $n(a) \propto a^{-3.5}$ (Mathis et al. 1977)   |
| Minimum grain size                 | $a_{\text{min}} = 0.005 \pm 0.003$ $\mu\text{m}$  |
| Maximum grain size                 | $a_{\text{max}} = 0.2 \pm 0.02$ $\mu\text{m}$   |
| Dust types                         | 95% warm silicates from Ossenkopf et al. (1992)<br>5% astronomical silicates from Draine & Lee (1984)                   |
| Optical depth                      | $\tau_{0.55\mu\text{m}} = 158 \pm 7$<br>$\tau_{2.2\mu\text{m}} = 6.5 \pm 0.3$<br>$\tau_{9.7\mu\text{m}} = 14.0 \pm 0.6$ |
| Radius                             | $R_{\star} \simeq 600 R_{\odot} = 2.79$ AU  |
| Radius of inner CDS boundary       | $R_{\text{in}} = 9.1 R_{\star} = 25.4$ AU   |
| Mass-loss rate                     | $\dot{M} = 2.18 \times 10^{-5} M_{\odot}/\text{yr}$   |
| Bolometric flux                    | $F_{\text{bol}} = 0.7 \times 10^{-10}$ W/m <sup>2</sup>   |

**Table 2.** The derived and adopted physical parameters of OH 104.9+2.4 as provided by Model M-II. Parameters that were treated as not time-dependent are indicated with \*. A distance of  $D = 2.38 \pm 0.24$  kpc (Herman & Habing 1985) and an outflow velocity of  $v_e = 15$  km s<sup>-1</sup> (te Lintel Hekkert et al. 1991) were assumed.

| Parameter                          |  | $\Phi = 0.5$<br>(1996) | $\Phi = 0$<br>(2002) | $\Phi = 0.25$<br>(2003) |
|------------------------------------|--|------------------------|----------------------|-------------------------|
| Black-body effective temperature   | $T_{\text{eff}}$ [K]                             | 2250                   | 3150                 | 2800                    |
| Temperature at inner CDS boundary* | $T_{\text{in}}$ [K]                              | 1000                   |                      |                         |
| Relative CDS thickness*            | $\frac{r_{\text{out}}}{r_{\text{in}}}$           | 10 <sup>5</sup>        |                      |                         |
| Minimum grain size*                | $a_{\text{min}}$ [ $\mu\text{m}$ ]               | 0.005                  |                      |                         |
| Maximum grain size*                | $a_{\text{max}}$ [ $\mu\text{m}$ ]               | 0.28                   |                      |                         |
| Dust-to-gas ratio*                 | $r_{\text{dg}}$                                  | 0.005                  |                      |                         |
| Dust grain bulk density*           | $r_s$ [g cm <sup>-3</sup> ]                      | 3.0                    |                      |                         |
| Optical depth                      | $\tau_{0.55\mu\text{m}}$                         | 146.7                  | 60.4                 | 103.6                   |
|                                    | $\tau_{2.2\mu\text{m}}$                          | 8.5                    | 3.5                  | 6.0                     |
|                                    | $\tau_{9.7\mu\text{m}}$                          | 13.9                   | 5.7                  | 9.8                     |
| Radius                             | $R_{\star}$ [ $R_{\odot}$ ]                      | 729                    | 675                  | 691                     |
|                                    | [AU]   | 3.39                   | 3.14                 | 3.21                    |
|                                    | [mas]  | 1.43                   | 1.32                 | 1.35                    |
| Radius of inner CDS boundary       | $R_{\text{in}}$ [ $R_{\star}$ ]                  | 8.3                    | 17.5                 | 13.7                    |
|                                    | [AU]   | 28.3                   | 55.0                 | 44.0                    |
|                                    | [mas]  | 11.9                   | 23.1                 | 18.6                    |
| Mass-loss rate                     | $\dot{M}$ [ $10^{-5} M_{\odot}/\text{yr}$ ]      | 3.09                   | 5.69                 | 5.17                    |
| Bolometric flux                    | $F_{\text{bol}}$ [ $10^{-10}$ W/m <sup>2</sup> ] | 0.7                    | 2.3                  | 1.5                     |
| Luminosity                         | $L$ [ $10^4 L_{\odot}$ ]                         | 1.23                   | 4.03                 | 2.63                    |
| Density profile within the CDS*    | radiatively driven wind                          | (Ivezić et al. 1999)   |                      |                         |
| Dust-grain distribution function*  | MRN, $n(a) \propto a^{-3.5}$                     | (Mathis et al. 1977)   |                      |                         |
| Dust type*                         | S99 cold silicates                               | (Suh 1999)             |                      |                         |

the dust composition used in M-I is the cold silicates from Suh (1999). With this dust type, we have found a model with an Ivezić et al. (1999) radiatively driven wind that gives a slightly better SED fit than corresponding models with  $\rho(r) \propto r^{-2}$ . In Fig. 3, the SED in the 10  $\mu\text{m}$  regime for M-I and the final M-II are shown for comparison.

The figure clearly illustrates how this new model is an improvement in this region. At this point, we would like to

note that the ISO SED of OH 104.9+2.4 shows some rather small emission features at 33.3  $\mu\text{m}$  and 40.6  $\mu\text{m}$ , which are not considered in detail by our model even with the updated (as compared to M-I) dust composition. Suh (2002) ascribes these features to crystalline silicates. However, it is difficult to extract information from those rather weak features and especially to positively identify them with specific dust components. Therefore, proper identification of these features may not

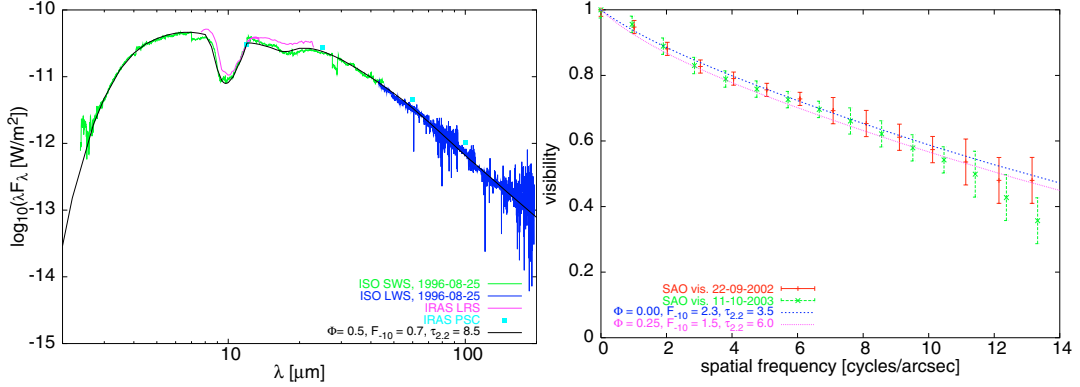


**Fig. 2.** SED (*left*) and  $2.12 \mu\text{m}$  visibility (*right*) of OH 104.9+2.4 for our best-fitting model M-II. In order to take into account the different epochs of the ISO (1996) and SAO (2002 & 2003) observations at  $2.12 \mu\text{m}$ , bolometric flux  $F_{\text{bol}}$ , optical depth  $\tau$ , and effective temperature  $T_{\text{eff}}$  had to be adjusted. The effective temperature of the central star is  $T_{\text{eff}} = 2250 \text{ K}$  for  $\Phi = 0.5$ ,  $T_{\text{eff}} = 3150 \text{ K}$  for  $\Phi = 0$ , and  $T_{\text{eff}} = 2800 \text{ K}$  for  $\Phi = 0.25$ .  $F_{-10}$  denotes the bolometric flux in  $10^{-10} \text{ W/m}^2$ , while  $\tau_{2.2}$  is the optical depth at  $2.2 \mu\text{m}$ .

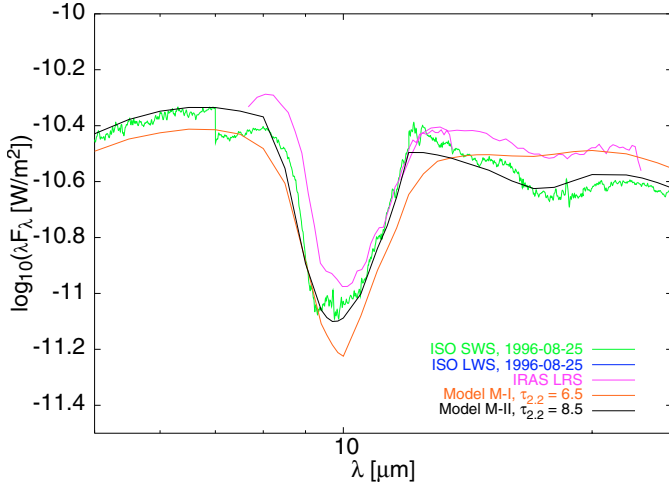


**Fig. 3.** SED of OH 104.9+2.4 in the mid-IR for models M-I (Paper I) and M-II (this work). Improvement in fitting the silicate absorption features is mainly due to the newly included dust composition.

be possible with current models. But, since these features are fairly weak, accounting for them in more detail would not significantly alter the conclusions of our study.

As we decided to use a model incorporating a radiatively driven wind, we had to comprehensively check our parameter sets to match the observed outflow velocities. The new best-fitting model results in an average terminal outflow velocity of  $v_e^{\text{M-II}} = 16.8 \text{ km s}^{-1}$ , which is in fair agreement with the observed outflow velocity of  $v_e = 15 \text{ km s}^{-1}$  from te Lintel Hekkert et al. (1991).

In addition, the effective temperature was adjusted to  $T_{\text{eff}} = 2250 \text{ K}$  for phase  $\Phi = 0.5$ . Considering the error bars found for M-I, this is only a minor adjustment.

### 3.2.2. Step 2: Fitting multiple pulsation phases

Comparing the 2002 and 2003 SAO visibility data, it is obvious that a simple rescaling of  $F_{\text{bol}}$  is insufficient for reproducing both observational constraints (SED and visibility) with a single model. The visibility scales with  $\sqrt{F_{\text{bol}}}$ , and the

difference in  $F_{\text{bol}}$  between the 2002 and the 2003 measurements is  $\Delta F_{\text{bol}} = 0.8 \times 10^{-10} \text{ W/m}^2$  (based on the assumption of a cosine-like pulsation phase, see Paper I), corresponding to 35% of  $F_{\text{bol}}^{\text{MAX}}$ . A difference of this order of magnitude cannot be derived from the SAO observations by merely rescaling the bolometric flux. Therefore, at least one additional parameter has to be changed to account for the observed variation of the visibility. To explain the observed change of depth for the  $9.7 \mu\text{m}$  absorption feature of other OH/IR stars, different authors have suggested a change in optical depth with pulsation phase (see Suh 2004, and references therein). With both proper scaling of  $F_{\text{bol}}$  as a function of the pulsation phase ( $\Phi^{2002} = 0$ ,  $F_{\text{bol}}^{2002} = 2.3 \times 10^{-10} \text{ W/m}^2$ ;  $\Phi^{2003} = 0.25$ ,  $F_{\text{bol}}^{2003} = 1.5 \times 10^{-10} \text{ W/m}^2$ ) and a linear adjustment of the optical depth ( $\tau_{2.2\mu\text{m}}^{\text{ISO}} = 8.5$ ,  $\tau_{2.2\mu\text{m}}^{2002} = 3.5$ ,  $\tau_{2.2\mu\text{m}}^{2003} = 6.0$ ), the 1996 ISO SED, as well as the 2002 and 2003 SAO visibilities, can be reproduced by a single model, as shown in Fig. 2.

Most detailed pulsation models for AGB stars predict an increase of  $T_{\text{eff}}$  between minimum and maximum pulsation phases. For Mira stars, Bessell et al. (1996) predict the maximum in  $T_{\text{eff}}$  to be at  $\Phi \approx 0.8$ . While radial pulsations of OH/IR stars are driven by the same mechanism, it is difficult to assess whether the same  $\Phi$ - $T_{\text{eff}}$ -relation is true for these objects. However, our primary interest is to find a suitable model that properly describes the relative changes between  $\Phi = 0.5$ ,  $\Phi = 0$ , and  $\Phi = 0.25$ . Based on Bessell et al. (1996) and taking into account that OH 104.9+2.4 is a cool star, we find  $T_{\text{eff}} = 2250 \text{ K}$  for  $\Phi = 0.5$ ,  $T_{\text{eff}} = 3150 \text{ K}$  for  $\Phi = 0$ , and  $T_{\text{eff}} = 2800 \text{ K}$  for  $\Phi = 0.25$  are appropriate to account for the phase-dependent change of the central star's effective temperature. Nevertheless, a change in  $T_{\text{eff}}$  has only a small impact on SED and visibility and almost the same effect as would a small adjustment of  $\tau$  in the opposite direction.

As can be seen from Table 2, the maximum grain size  $a_{\text{max}}$  was increased for this model as compared to M-I. The new value of  $a_{\text{max}} = 0.28 \mu\text{m}$  for M-II deviates from  $a_{\text{max}} = 0.20 \mu\text{m}$  for M-I by  $4\sigma$ , but the change was necessary in order to enable us to scale the optical depth properly. This does not come as a surprise, since, changing two different parameters in opposite directions may lead to nearly identical models,

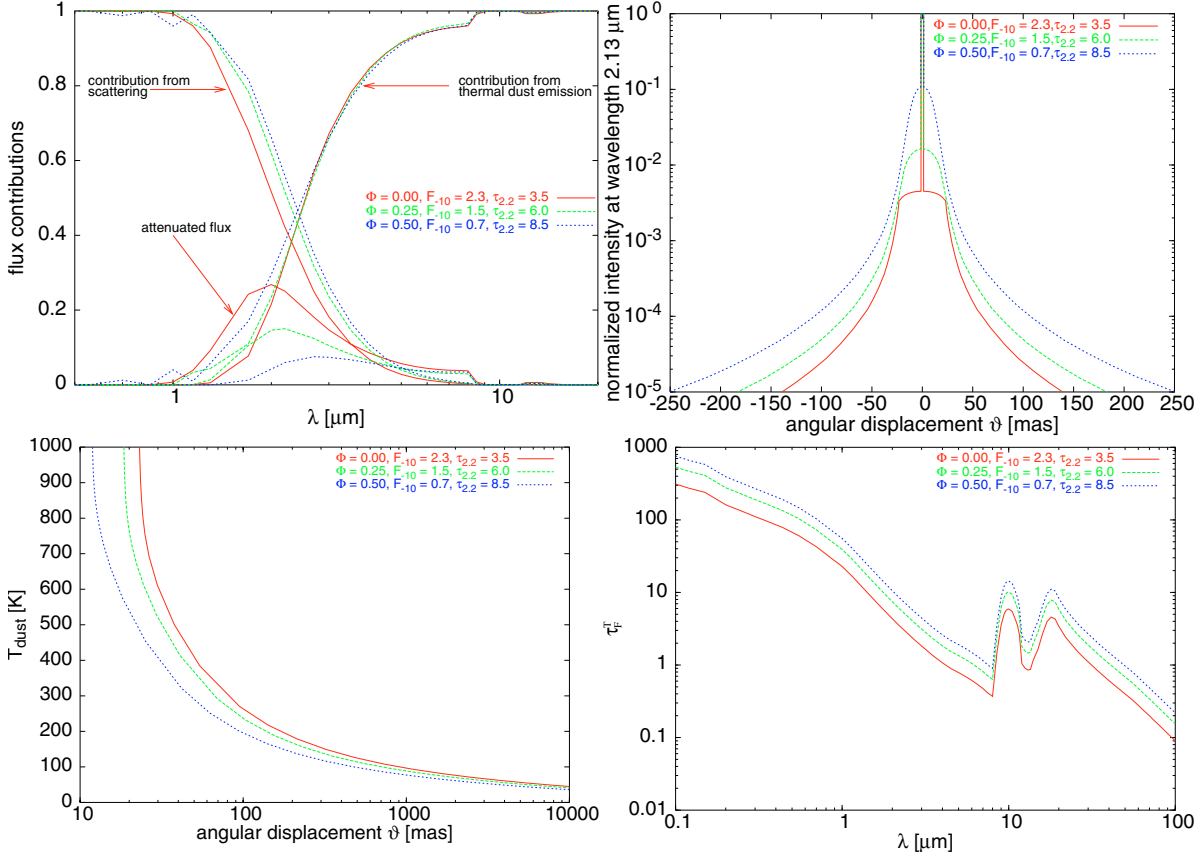


**Fig. 4.** Modeling results of OH 104.9+2.4 for our best-fitting model M-II at the pulsation phases of the observations (see Table 2). *Top left:* fractional contributions to the total flux. The contribution from direct stellar light is small compared to the contribution of dust scattering and thermal emission to the physical processes in the CDS (see Table 3). *Top right:* the normalized intensity profile at 2.13  $\mu\text{m}$ . The sharp central peak corresponds to the central source of radiation. *Bottom left:* dust temperature as a function of angular distance. The point where  $T_{\text{dust}} = 1000$  K indicates the inner radius of the dust shell. As the figure shows, due to the variability of the central source, the inner dust shell boundary moves from 11.9 mas to 23.1 mas from minimum to maximum pulsation phase. *Bottom right:* wavelength dependence of the total optical depth.

as pointed out in Paper I. Therefore, we were able to find different models of similarly good quality in Paper I. The new best-fitting model M-II is much more constrained by observations than M-I, as the third observational constraint turned out to be essential in order to show the necessity of adjusting the optical depth for different phases of OH 104.9+2.4.

Concerning the 2003 SAO visibility, M-II cannot reproduce the observations beyond 12 cycles/arcsec very well. This may be due to the large observational errors close to the diffraction limit, which are possibly slightly underestimated by the error bars shown here, as there is no obvious physical reason why the visibility curvature should change as drastically as suggested by Fig. 2 in that regime between the dates of the two SAO observations.

### 3.2.3. Further model results

The top left panel of Fig. 4 shows the fractional flux contributions of the emerging stellar radiation, scattered radiation, and thermal dust emission as a function of wavelength for model M-II. At 2.2  $\mu\text{m}$ , the flux is dominated by scattered light for all phases (see Table 3). The contribution of direct

**Table 3.** The contributions to the total flux at 2.2  $\mu\text{m}$  for different pulsation phases  $\Phi$  as given by Model M-II.

| Component  | $\Phi = 0.5$ | $\Phi = 0$ | $\Phi = 0.25$ |
|------------|--------------|------------|---------------|
| Attenuated | 5.9%         | 25.1%      | 15.0%         |
| Scattering | 55.9%        | 42.2%      | 51.7%         |
| Thermal    | 38.2%        | 32.7%      | 33.3%         |

stellar light (attenuated flux) rises from  $\sim 6\%$  at minimum phase to  $\sim 25\%$  at maximum phase.

The top right panel of Fig. 4 shows the normalized intensity distribution at 2.13  $\mu\text{m}$  as a function of angular distance. The barely resolved central peak corresponds to the central star. Here, the increase in the flux contribution of the central source towards maximum phase is reflected by the rise of the central peak, as it does indeed become larger. In addition, the inner rim of the CDS itself moves outwards.

The bottom left panel of Fig. 4 shows a plot of the dust temperature as a function of angular distance. The inner CDS radius  $r_{\text{in}}$  can be derived directly from the radial profile, as it is the point at which the dust reaches  $T_{\text{in}} = 1000$  K. It corresponds to an angular radius of  $\vartheta_{\text{in}} = 11.9$  mas for  $\Phi = 0.5$

(for M-I:  $\vartheta_{\text{in}} = 10.5$  mas),  $\vartheta_{\text{in}} = 18.6$  mas for  $\Phi = 0.25$ , and  $\vartheta_{\text{in}} = 23.1$  mas for  $\Phi = 0$ . This again shows that the inner rim of the CDS moves outwards as the pulsation phase rises from minimum to maximum, mainly a consequence of increasing  $L_{\star}$ . According to our model, the change in the inner dust shell radius between minimum and maximum phases is approximately a factor of two.

The bottom right panel of Fig. 4 shows the total optical depth as a function of wavelength. As can be expected for the chosen chemical composition, local maxima of  $\tau_{\lambda}$  are found for the silicate absorption features at  $9.7 \mu\text{m}$  (SiO stretching vibrations) and  $18 \mu\text{m}$  (SiO<sub>2</sub> bending vibrations). The shape of the profile remains the same for all pulsation phases, but the optical depth is higher for all wavelengths towards the minimum pulsation phase.

The stellar radius drops by 8% between minimum and maximum phases (from  $729$  to  $675 R_{\odot}$ ), which is consistent with the Stefan-Boltzmann law. The radius at  $\Phi = 0.5$  is approximately 18% larger as compared to the value derived for M-I. As described in Paper I, the mass-loss rate  $\dot{M}$  can be calculated using the observed outflow velocity  $v_e = 15 \text{ km s}^{-1}$  and our derived luminosities for the different phases (see Table 2). For minimum phase,  $\dot{M} = 3.09 \times 10^{-5} M_{\odot}/\text{yr}$  is obtained, which is roughly 50% larger than the value found for M-I. For maximum phase, we derive  $\dot{M} = 5.69 \times 10^{-5} M_{\odot}/\text{yr}$ , which is by a factor of 1.8 larger than the mass-loss rate at minimum pulsation phase. Heske et al. (1990) found  $\dot{M} = 5.58 \times 10^{-5} M_{\odot}/\text{yr}$ , which is in good agreement with our result.

### 3.3. Quality of the SED modeling at different phases

In Sect. 3.2 it was shown that model M-II is able to properly reproduce the ISO SED and the SAO visibilities. But, as argued in Paper I, the SED varies in overall flux as well as in shape, depending on the pulsation phase. Therefore, this has to be tested if M-II is to reproduce the SED of OH 104.9+2.4 at different pulsation phases. Unfortunately, only few photometry is available besides the ISO spectrum at minimum phase; while for some data, the pulsation phase is uncertain, as the observing date is not specified in the corresponding publications. Therefore, we decided to perform only a qualitative test on the data used in Paper I to derive the SED at maximum phase. Figure 5 shows the results. The models at minimum and maximum phase properly constrain the range of observational data. Thus, Model M-II seems to correctly reproduce the change in shape and the scaling with  $F_{\text{bol}}$  of the SED of OH 104.9+2.4.

## 4. Summary and conclusions

We present an improved, quasi-time-dependent radiative transfer model for the dust shell of the type II-A OH/IR star OH 104.9+2.4. This model is constrained by recent speckle-interferometric observations at  $2.12 \mu\text{m}$  and by spectrophotometric observations. The speckle observations were carried out with the SAO 6 m telescope at a diffraction-limited resolution of  $74$  mas, which is sufficient for resolving the CDS at this wavelength. The reconstructed 2-dimensional visibility shows no major deviation from spherical symmetry.

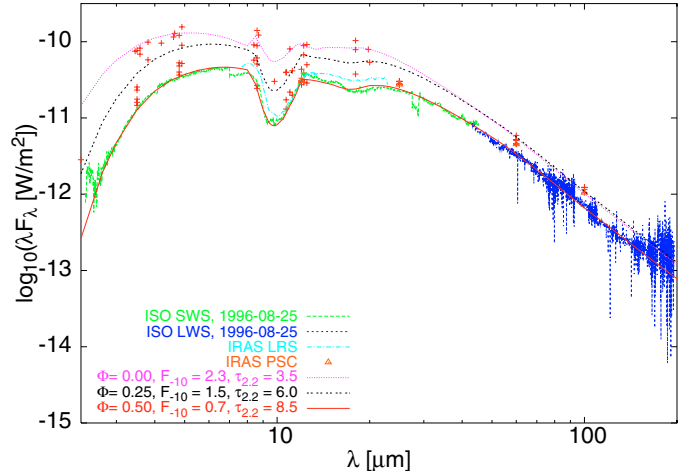


**Fig. 5.** Variation of the SED with pulsation phase. All data collected in Paper I (see Fig. 2 in Paper I, and references therein) are plotted in order to test the quality of the SED fit of M-II for the 2002/2003 visibility phases.

As a reference SED, we used the ISO SWS and LWS spectra ( $\lambda = 2.38\text{--}196 \mu\text{m}$ ) from 1996, which correspond to minimum pulsation phase, as well as additional photometric data at different phases (see Paper I for details).

Our simultaneous modeling of visibilities at different pulsation phases and of the ISO SED of OH 104.9+2.4 lead to modifications of our previous best-fitting model presented in Paper I. The new results demonstrate the need to consider changes in bolometric flux, as well as in optical depth and central star effective temperature with pulsation phase, in order to obtain more reliable results.

The final best-fitting model of this study leads to prediction of a temperature at the inner rim of the dust shell of  $T_{\text{in}} = 1000$  K. The dust shell has a relative thickness of  $10^5$ , while the density decreases outwards according to a radiatively driven wind as described in Ivezić et al. (1999). The dust grains follow a standard MRN distribution with grain sizes  $a = 0.005\text{--}0.28 \mu\text{m}$ , while the optical constants of the dust itself are represented best by the cold silicates from Suh (1999). The optical depth varies between minimum and maximum pulsation phase from  $\tau_{2.2\mu\text{m}} = 8.5$  to  $\tau_{2.2\mu\text{m}} = 3.5$ , while the bolometric flux changes from  $F_{\text{bol}} = 0.7 \times 10^{-10} \text{ W/m}^2$  to  $F_{\text{bol}} = 2.3 \times 10^{-10} \text{ W/m}^2$ .

Based on pulsation models for Mira stars (Bessell et al. 1996), variation of the effective temperature of the central star with pulsation phase is taken into account. For the cool star OH 104.9+2.4, the best-fitting model predicts a change from  $T_{\text{eff}} = 2250$  K to  $T_{\text{eff}} = 3150$  K between minimum and maximum pulsation phases. While a change in  $T_{\text{eff}}$  shows only a minor impact on SED and/or visibility, it leads to a prediction of the change in the stellar radius (from  $R_{\star} = 729 R_{\odot}$  at minimum phase to  $R_{\star} = 675 R_{\odot}$  at maximum phase) for our best-fitting model, which is in agreement with observations of similar objects (see, e.g., Bessell et al. 1996). The inner rim of the dust shell moves outwards by roughly a factor of two from minimum to maximum phase ( $R_{\text{in}} = 28.3\text{--}55.0$  AU), while an increase of the mass-loss rate from  $\dot{M} = 3.09 \times 10^{-5} M_{\odot}/\text{yr}$  to

$\dot{M} = 5.69 \times 10^{-5} M_{\odot}/\text{yr}$  is found. Several observational constraints (1996 ISO SED, 2002/2003 SAO visibilities, IR photometry at different epochs) are represented very well by this model. Only the 2003 visibility at high spatial frequencies shows deviation from the model, which may be due to underestimation of observational errors.

In the future, it would be very important to obtain  $K'$ -band visibility measurements at pulsation phase  $\Phi = 0.5$  in order to check the validity of the phase-dependent model, although conclusions may be limited due to possible cycle-to-cycle variations. Additional measurements for intermediate phases would help to check if the optical depth really scales linearly with the pulsation amplitude or if a more complex approach has to be considered. Likewise, it is still necessary to carry out more photometric measurements in order to pin down the pulsation period with higher precision. Furthermore, visibilities at other wavelengths (probably  $J$  or  $H$ , which poses a challenge due to the detection limit) would help to improve the modeling and would give more detailed information on the spatial structure of the dust shell.

*Acknowledgements.* We thank the Infrared Space Observatory (ISO) operators at the European Space Agency (ESA) for providing the SED data. This research has made use of the SIMBAD database operated by CDS in Strasbourg as well as the Gezari catalogue published by the National Aeronautics and Space Administration (NASA), and the NASA Astrophysics Data System (ADS) operated

by NASA. This publication makes use of data products from the Two Micron All Sky Survey (2MASS), which is a joint project of the University of Massachusetts and the Infrared Processing and Analysis Center/California Institute of Technology, funded by NASA and the National Science Foundation. A.B.M. acknowledges support from the Natural Sciences and Engineering Research Council of Canada (NSERC). Finally, we thank the anonymous referee for helpful comments that stimulated further improvements in the manuscript.

## References

- Bessell, M. S., Scholz, M., & Wood, P. R. 1996, *A&A*, 307, 481  
 Draine, B. T., & Lee, H. M. 1984, *ApJ*, 285, 89  
 Habing, H. J. 1996, *A&AR*, 7, 97  
 Herman, J., & Habing, H. J. 1985, *A&AS*, 59, 523  
 Heske, A., Forveille, T., & Omont, A. 1990, *A&A*, 239, 173  
 Ivezić, Z., Nenkova, M., & Elitzur, M. 1999, Internal Report, Univ. of Kentucky  
 Labeyrie, C. D. 1970, *A&A*, 6, 85  
 Mathis, J. S., Rimpl, W., & Nordsieck, K. H. 1977, *ApJ*, 217, 425  
 Ossenkopf, V., Henning, T., & Mathis, J. S. 1992, *A&A*, 261, 567  
 Riechers, D., Balega, Y., Driebe, T., et al. 2004, *A&A*, 424, 165 (Paper I)  
 te Lintel Hekkert, P., Caswell, J. L., Habing, H. J., Haynes, R. F., & Norris, R. P. 1991, *A&AS*, 90, 327  
 Suh, K.-W. 1999, *MNRAS*, 304, 389  
 Suh, K.-W. 2002, *MNRAS*, 332, 513  
 Suh, K.-W. 2004, *ApJ*, 615, 485